Chemical Engineering Journal 431 (2022) 134109

Contents lists available at ScienceDirect

Chemical Engineering Journal

journal homepage: www.elsevier.com/locate/cej

A PEDOT:PSS conductive hydrogel incorporated with Prussian blue nanoparticles for wearable and noninvasive monitoring of glucose

Changshun Xu [a,b,1], Danfeng Jiang [a,b,c,1], Yuancai Ge [a,b], Liping Huang [a,b], Yang Xiao [c], Xueqian Ren [a,b], Xiaohu Liu [a,b], Qingwen Zhang [a,b,c,*], Yi Wang [a,b,c,*]

[a] School of Biomedical Engineering, School of Ophthalmology and Optometry, Eye Hospital, Wenzhou Medical University, Wenzhou 325001, PR China
[b] Oujiang Laboratory (Zhejiang Lab for Regenerative Medicine, Vision and Brain Health), Wenzhou 325001, PR China
[c] Engineering Research Center of Clinical Functional Materials and Diagnosis & Treatment Devices of Zhejiang Province, Wenzhou Institute, University of Chinese Academy of Sciences, Wenzhou 325001, PR China

ARTICLE INFO

Keywords:
Glucose
PEDOT:PSS
Prussian blue
Electrochemical sensors

ABSTRACT

Currently, there is no commercially-available noninvasive method for glucose monitoring in the interstitial fluid (ISF) mainly due to the measurement accuracy, sensitivity and/or the weak blood correlation. Here, we present an electrochemical biosensor based on PEDOT:PSS conductive hydrogel incorporated with Prussian blue nanoparticles (PBNPs) for the noninvasive and continuous monitoring of glucose on body. The hydrogel was prepared with the addition of dimethyl sulfoxide (DMSO) and Zonyl FS-300, which helped to improve the expanding of the polymer chains for the formation of better conductive and nanoporous networks. The hydrogel-based biosensor showed a low detection limit of 0.85 μM for glucose detection and high sensitivity up to 340.1 $\mu A\cdot mM^{-1}\cdot cm^{-2}$, which was about 10-fold higher than the counterparts based on agarose and hydroxyethyl methacrylate (HEMA) hydrogels. Furthermore, it provided good accuracy with commercial glucometer for the glucose detection in serum. More importantly, incorporated with the reverse iontophoresis (RI), the hydrogel was applied as a skin patch on human subject for the *in vivo* noninvasive and continuous monitoring of ISF-borne glucose. The results showed good correlation with that measured by blood glucometer. We believe such glucose biosensor paves the way to clinically wearable noninvasive glucose monitoring in diabetics.

1. Introduction

Diabetes mellitus is a metabolic disorder of multiple aetiology characterized by hyperglycaemia which can cause many serious complications, including blindness, renal failure and neuropathy [1]. Frighteningly, the number of diabetic patients is rapidly increasing and the total number will reach to 578 million according to the report from World Health Organization [2]. Diabetes is not completely curable and control the level of blood glucose is considered the crutial for diabetes [3–5]. The current widespread method for the glucose detection is based on the self-testing blood glucose meters, which rely on the inconvenient and painful blood sampling from the finger tip. Other several cormercially avilable systems include minimally invasive microneedle sensors which are inserted under the skin for the measurement of interstitial fluid glucose. However, they are all based on the invasive detection. Thus, completely noninvasive detection method with the ability of continous monitoring of glucose level would be ideal for diabetes magnagement. Therefore, various methods for noninvasive detection of glucose in blood and other biofluids (such as saliva, sweat, tears and interstitial fluid (ISF)) have been developed, such as near-infrared relectance spectroscopy [6,7], optical coherence tomography [8], colorimetry [9,10], photonic crystal spectrometer [11], piezoelectrical sensing [12], Raman spectroscopy [13], microwave methods [14] and electrochemical technology [15–17]. Among these methods, electrochemical technology has received extensive interests due to the attractive properties of low cost, simple, quantitative and ease of miniaturization for wearable and porable devices [18,19]. Electrochemical method has showed the feasibility for the continous monitoring of sweat glucose [20] which however has weak correlation to the blood glucose. Other noninvasive glucose monitoring includes the

* Corresponding authors at: School of Biomedical Engineering, School of Ophthalmology and Optometry, Eye Hospital, Wenzhou Medical University, Wenzhou, 325001, PR China.

E-mail addresses: zhangqw@wiucas.ac.cn (Q. Zhang), wangyi@wiucas.ac.cn (Y. Wang).

[1] Changshun Xu and Danfeng Jiang contributed equally to this work.

https://doi.org/10.1016/j.cej.2021.134109
Received 29 July 2021; Received in revised form 4 November 2021; Accepted 8 December 2021
Available online 13 December 2021
1385-8947/

electrochemical method incorporated with reverse iontophoresis (RI) technique for the extraction of ISF glucose to the surface of skin followed by the detection via electrochemical sensor [21,22]. In this method, a thin hydrogel layer was typically applied on the electrode to improve the contacts between the electrode and skin and provide a stroage for glucose reaction with the glucose oxidase (GOx). However, the concentration of extracted ISF glucose is about 2 to 3-fold lower (i.e. μM level) than the blood glucose, while the hydrogel with poor conductivity may hindered the electron transfer to electrode thus limited the sensitivity. Therefore, to achieve an accurate sensing result, it is necessary to have sensing material with strong electrocatalysis and a highly conductive hydrogel as the contact layer for highly sensitive electrochemical glucose sensor [23].

Considered as an “artificial peroxidase”, prussian blue (PB) has been reported with an outstanding electrocatalytic activity up to three orders of magnitude higher than platinum for the catalysis of hydrogen peroxide (H_2O_2), the byproduct of enzymatic reaction [24–26]. Therefore, it has been widely applied in the construction of glucose sensors [27–29]. However, the weak conductivity of PB may hinder the electron transports thus reduce the sensitivity for glucose detection. To overcome this deficiency, some highly conductive materials including nobel metals and carbon materials have been introduced such as Ag nanowires [30], graphene [31], carbon nanotubes [32], poly (3,4-ethylenedioxythiophene):poly (styrene sulfonate) (PEDOT:PSS) [33], and other conducting polymers [34]. Among these materials, PEDOT:PSS offered the advantages of good conductivity, high flexibility and stretchability. The PEDOT:PSS provides the promising conductivity and extensive electron transport paths due to the π-π conjugation [35]. It has been widely empolyed for fabricating many kinds of sensing devices including strain, pressure, temperature sensors, and biosensors [36-39]. Interestingly, the PEDOT:PSS can also be prepared as a soft hydrogel matrix supporting the incorporation of other functional materials such as insulating elastomers [40]. Futhermore, the good biocompatibility of PEDOT:PSS hydrogel are also crutial for wearable applications where the direct contact with human body require comfort and good contacts between the skin and electrode [40,41].

In this work, we prepared an ultra sensitive noninvasive electrochemical glucose sensor with the composite hydrogel electrode which incorporated PB nanoparticles (PBNPs) with the conducting PEDOT:PSS hydrogel. The PEDOT:PSS hydrogel was employed as a skin patch for the improvement of contact between the sensor and the skin, while its high conductivity may contribute to the achievement of high sensitivity. Dimethyl sulfoxide (DMSO) and Zonyl FS-300 were mixed with the PEDOT:PSS solution to form the homogeneous hydrogel solution with better expanded polymer chains. The PBNPs and glucose oxidase (GOx) were embedded into the hydrogel solution followed by the modification

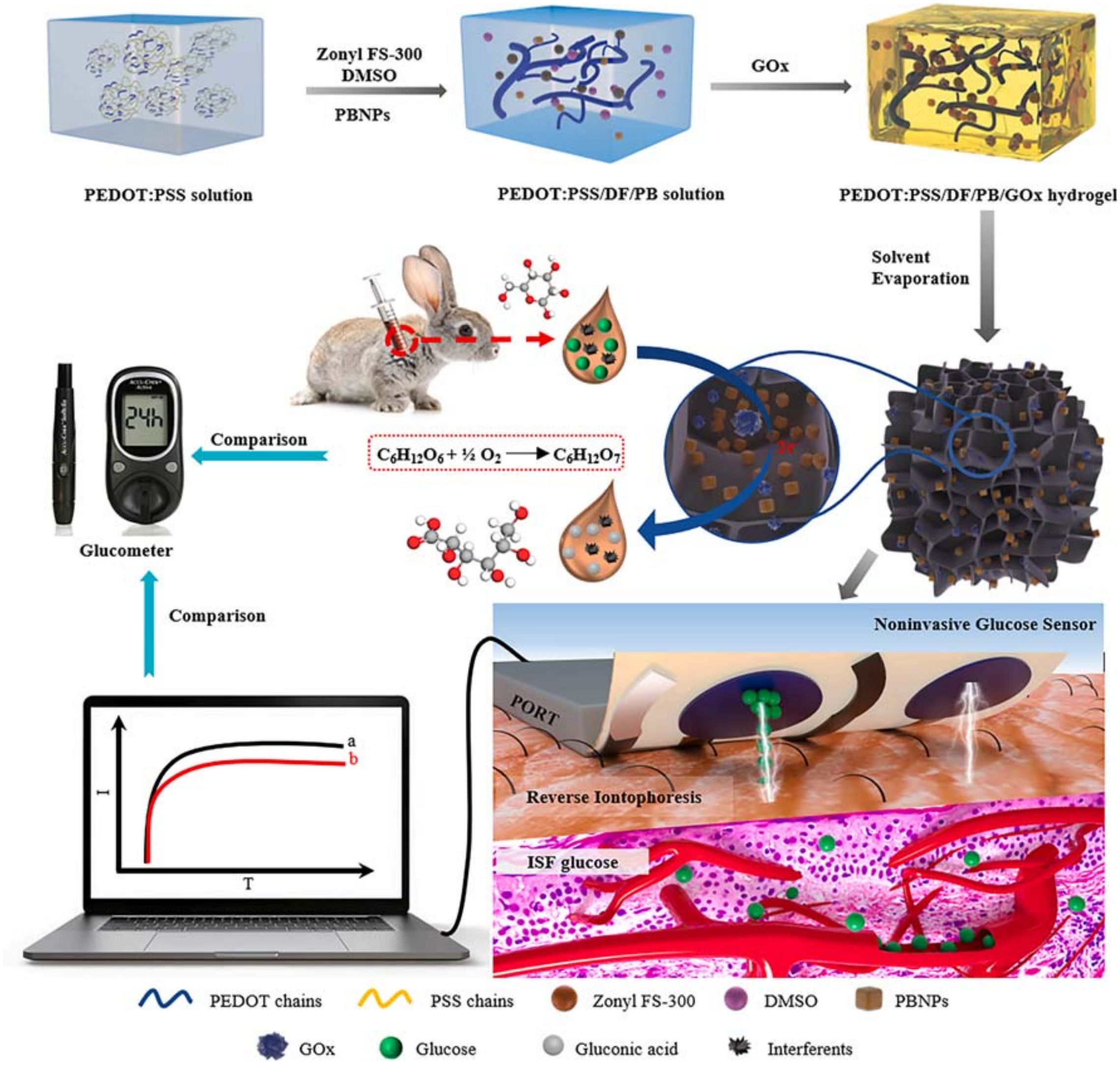

Fig. 1. The schematic demonstration on the preparation of PEDOT:PSS/DF/PB/GOx sensor for the glucose detection in serum and the noninvasive ISF glucose detection on human skin based on the reverse iontophoresis (RI), along with comparison to the glucose measurement by commercial glucometer.

on the electrode and solvent evaporation, which results into the formation of glucose sensing films (Fig. 1). A three dimensional honeycombed morphology of sensing film supported to supply numerous electron transport paths and abundant active sites for the loading of PBNPs. We compared the sensitivity of PEDOT:PSS hydrogel with other nonconductive hydrogel such as agarose and hydroxyethyl methacrylate (HEMA) based hydrogel, which were reported as the skin patch on the RI-extraction based noninvasive ISF glucose detection. The cylic voltammetry (CV) and chronoamperometry tests of the glucose sensor were carried out in the PBS and rabbit serum. The performance of the sensor was evaluated for the detection of glucose in serum and compared with the commercial glucometer. Furthermore, the sensor was applied on two volunteers' skin for the continuously noninvasive ISF glucose monitoring up to 15 h with snack intaken. The results were synchronously compared with the blood glucose measured by the finger-stick blood sampling.

2. Experiments

2.1. Reagents and apparatus

PEDOT:PSS (Clevios PH1000) was purchased from Heraeus. The PEDOT:PSS contained 1–1.3% colloidal gel with the weight ratio of PEDOT and PSS at 1:2.5. Glucose, uric acid (UA), dopamine (DA), hydrogen peroxide solution (H_2O_2, 30%), sodium chloride (NaCl) were purchased from Shanghai Macklin Biochemical Co., Ltd. Potassium ferricyanide ($K_3Fe(CN)_6$) and iron(III) chloride hexahydrate ($FeCl_3 \cdot 6H_2O$), ascorbic acid (AA) were received from Shanghai Aladdin Bio-Chem Technology Co., Ltd. Hydrochloric acid (HCl, 30%) was obtained from Shanghai Lingfeng Chemical Reagent Co. Ltd. (China). Dimethyl sulfoxide (DMSO), Zonyl FS-300, 2-hydroxyethyl methacrylate (HEMA), ethylene glycol dimethacrylate (EGDMA), 2-hydroxy-2-methyl-1-phenyl-1-propanone (HMPP), agarose, glucose oxidase (GOx) from *Aspergillus niger* (E.C.1.1.3.4, 158,200 U/g) were purchased from Sigma-Aldrich. Rabbit serum was obtained from Beijing Huaaokean Technology Co., Ltd. Glass carbon electrode (GCE), Pt wire and Ag/AgCl (saturated KCl) electrode were received from Shanghai Chuxi Industry Co., Ltd. Glucometer was purchased from ACON Laboratories, Inc.

Field emission scanning electron microscope (FESEM, Hitachi, SU8010) and Field emission transmission electron microscopy (FETEM, F200S) were employed to characterize the morphology and structures of the prepared materials. Fourier-transform infrared (FTIR, Tensor II, USA) was employed to prove the constituents of hydrogel related materials. All of electrochemical measurements were carried out in a 0.05 M phosphate buffered saline (PBS, pH 7.4) containing 0.1 M KCl by using electrochemical workstation (CHI 660E, Shanghai Chenhua Instrument Co., Ltd). Zeta potential measurements of PBNPs and PEDOT:PSS solution were carried out by Coulter Counter (Beckman Coulter, Multisizer 4e, USA).

2.2. Preparation of PBNPs and PB modified GCE electrode

The PBNPs were prepared according to our previously published paper with minor modifications [42]. Briefly, the PBNPs was synthesized by the chemical reaction of two mixed solutions labeled as solution A and B. Solution A contained 0.01 M $K_4[Fe(CN)_6]$, 0.1 M KCl and 0.1 M HCl in deionized (DI) water. Solution B was prepared by dissolving $FeCl_3$ (0.01 M), KCl (0.1 M) and HCl (0.1 M) in DI water. Subsequently, 150 mL solution A and 150 mL solution B were added separately into 100 mL water at a speed of 1000 μL/min with syringes and kept in the water bath at 35 ℃. After the synthesis, the precipitation was collected with centrifugation at rate of 6000 r/min and dried at 60 ℃ overnight for further use.

The PB modified GCE electrode (diameter of 3 mm) was fabricated by dropping 1 μL 50 mg/mL PBNPs dispersion on GCE surface and dried at room temperature.

2.3. Fabrication of PEDOT:PSS/DF/PB modified GCE electrodes

Firstly, PEDOT: PSS, DMSO and Zonyl FS-300 (PEDOT:PSS/DF) were mixed with the volume ratio of 94:5:1. Then, the mixed solution was stirred vigorously overnight at room temperature and stored at 4℃ for further use. In order to optimize the content of PBNPs, the PBNPs with different mass fractions of 2.5 %, 5%, 10% and 15% were respectively mixed with the above solution to form four kinds of PEDOT:PSS/DF/PB solution.

The PEDOT:PSS/DF/PB GCE electrodes were fabricated by dropping 1 μL of the PEDOT:PSS/DF/PB solution on the GCE surface and dried at room temperature. Four different PEDOT:PSS/DF/PB GCE were obtained with PBNPs of 2.5 %, 5%, 10% and 15% in mass fraction, respectively.

The control electrode of PEDOT:PSS/PB GCE was fabricated similarly at the absence of DMSO and Zonyl FS-300 solution. The control electrode of PB/GCE electrode was fabricated by drop-casting 1 μL of the solution containing 5% mass fractions of PBNPs.

2.4. Fabrication of PEDOT:PSS/DF/PB/GOx sensor

The GOx enzyme was immobilized in the PEDOT:PSS/DF/PB hydrogel electrode by two methods, drop-coating and embedding. For the drop-coating of GOx, 1 μL PEDOT:PSS/DF/PB hydrogel was first formed on the GCE. Then, 1 μL of GOx solution (20 mg/ml GOx dissolved in 0.5% glutaraldehyde) was dropped on the above PEDOT:PSS/DF/PB GCE electrode surface to form the sensing film for further use. For the embedding method, GOx was mixed homogeneously in PEDOT:PSS/DF/PB solution before dropped-coated on the GCE electrode. The pH of PEDOT:PSS/DF/PB solution was firstly adjusted from 4, 5, 5.5, 6 to 7 by adding 0.1 M NaOH prior to mix with 20 mg/mL GOx solution. Finally, 1 μL of the mixed solution with different pH values were dropping-coated on the GCE electrode and dried at room temperature for further study. The PEDOT:PSS/DF/PB/GOx film was formed upon the evaporation of the solvent.

For the noninvasive on-body glucose monitoring, the screen-printed carbon electrodes (SCPE) on PET substrate were prepared as the working electrode and counter electrode, and the Ag/AgCl electrode was fabricated as the reference electrode. In addition, a reverse iontophoresis (RI) electrode with diameter of 1 cm was prepared with SCPE. On the working electrode and the RI electrode, 11 μL of above prepared PEDOT:PSS/DF/PB solution (with 5 wt% of PBNPs) were drop-coated, respectively, and dried to form a uniform conductive hydrogel layer.

As the control experiments, the HEMA/PB/GOx GCE and agarose/PB/GOx GCE were also prepared similarly by mixing the GOx with HEMA and agarose solution before the formation of hydrogel for the sensing applications. The HEMA/PB/GOx GCE was prepared according to a previously reported literature [43]. Firstly, 50 mg PBNPs, 20 mg GOx, 1 mL polymer monomer 2-hydroxyethyl methacrylate (HEMA), 15 μL cross-linker ethylene glycol dimethacrylate (EGDMA, 80 mM) and 9.5 μL photo-initiator 2-hydroxy-2-methyl-1-phenyl-1-propanone (HMPP, 1% w/v) were added into a tube and dissolved by ultrasonication. During these processes, the tube was protected from light. Secondly, 1 μL of the final precursor solution was added on the surface of GCE and treated with UV irradiation at the intensity of 22 mW/cm^2 for 40 min at room temperature to form the HEMA/PB/GOx GCE. For the agarose/PB/GOx GCE, 50 mg PB, 40 mg agarose and 1 mL water were added into glass bottle and dissolved by heating under 100 ℃. The solution was stored in oven under 60 ℃ for 30 min, followed by addition of 20 mg GOx. Finally, 1 μL of the above solution was added into the surface of GCE and cooled to the room temperature to form agarose/PB/GOx GCE.

2.5. Electrochemical measurements

All electrochemical measurements were carried out by electrochemical workstation (CHI 660E) with conventional three-electrode system. Cyclic voltammetry (CV) and chronoamperometry tests were performed in the 0.05 M PBS (pH = 7.4). *I-t* curves were obtained at working potential of −0.05 V by the successive addition of 4 μL 10 mM glucose solution into 40 mL PBS, while serum sample detection was conducted by adding 200 μL serum into 40 mL PBS. Electrochemical impedance spectroscopy (EIS) was performed in the solution containing 5 mM $[Fe(CN)_6]^{4-/3-}$ (1:1) and 0.1 M KCl. The frequency was set at a range from 0.1 Hz to 1000 kHz, with the initial test voltage of −0.05 V and amplitude of 5 mV. An Ag/AgCl (saturated KCl) electrode and a Pt wire were utilized as the reference electrode and the counter electrode, respectively.

The interference experiments were also carried out in different interferents including ascorbic acid (AA, 10 μM), uric acid (UA, 100 μM), NaCl (100 μM), acetaminophen (AP, 100 μM) in 0.05 M PBS solution, respectively. The time dependent current response of PEDOT:PSS/DF/PB/GOx biosensor were recorded in real-time during the detection of different interferents.

The sensitivity, long-term stability, reproducibility of PEDOT:PSS/DF/PB/GOx sensor were implemented by the successive addition of 4 μL 10 mM glucose solution into the PBS solution at −0.05 V working potential.

2.6. On-Body glucose monitoring

The on-body glucose monitoring was performed with a protocol approved by the institutional review board (IRB) at School of Biomedical Engineering, School of Ophthalmology and Optometry, Wenzhou Medical University (2021-J-42). Two healthy volunteers with no prior medical history of heart conditions, diabetes, or chronic skeletomuscular pain, were recruited for participation in the study. The subjects were requested to arrive at the lab in a fasting state. The glucose sensor electrodes were attached on the skin, and a control measurement was achieved by recording the amperometric *I-t* response at a potential of −0.05 V (vs Ag/AgCl) for 5 min to obtain the curve "a". Afterwards, a potential of −3 V was applied between the working electrode and the RI electrode for 10 min to extract ISF glucose to the surface of the skin. Finally, the amperometric *I-t* measurement was carried out at a potential of −0.05 V (vs Ag/AgCl) for 5 min to achieve the curve "b". The current difference between curve "b" and "a" at 100 s was recorded as the glucose response signal. The detection was performed at every hour and the subjects were asked to take a snack with about 90 g of sugar (similar with the glucose tolerance test) in a specific time to investigate the blood glucose variations. For each glucose test, finger-stick blood measurements were performed as comparison at 15-min before the ISF extraction using commercial glucose strips (On·Call) to establish the correlation between the response of noninvasive ISF glucose and the blood glucose level.

3. Result and discussion

3.1. Characterization of PEDOT:PSS/DF/PB hydrogel

As shown in Fig. 1, the PEDOT:PSS/DF/PB/GOx sensor has been developed for the monitoring of glucose in the serum. It has to be noted that the conductivity of PEDOT:PSS is limited by the internal disconnected polymer chains. In order to obtain stronger electron transfer ability, DMSO and Zonyl FS-300 were introduced into PEDOT:PSS solution as exhibited in Fig. 1. These two materials enabled the polymer chains of PEDOT to better expand for the formation of conducting network [35]. The PBNPs were employed to catalyze H_2O_2 while PEDOT:PSS was acted as a conducting network for rapid electron transfer. In oder to obtain higher electric response, the distribution of PBNPs was optimized in the PEDOT:PSS hydrogel. The morphologies of PBNPs and PEDOT:PSS/DF/PB hydrogel were characterized by SEM in Fig. 2a–c. The PBNPs showed the size between 50 nm and 100 nm in Fig. 2a. According to the zeta potential measurements (Fig. S1, Supporting Information), the PBNPs were negatively charged (–33 mV) which can attract to the positively charged EDOT polymer (monomer of PEDOT, 0.25 mV). Interestingly, the PEDOT:PSS/DF hydrogel showed typical honeycombed structure with numerous nanosheets which provided large space sites for the immobilization of PBNPs (Fig. 2b). In Fig. 2c inset, it showed the PBNPs closely attached on the surface of PEDOT:PSS nanosheets with a uniform distribution. From the TEM

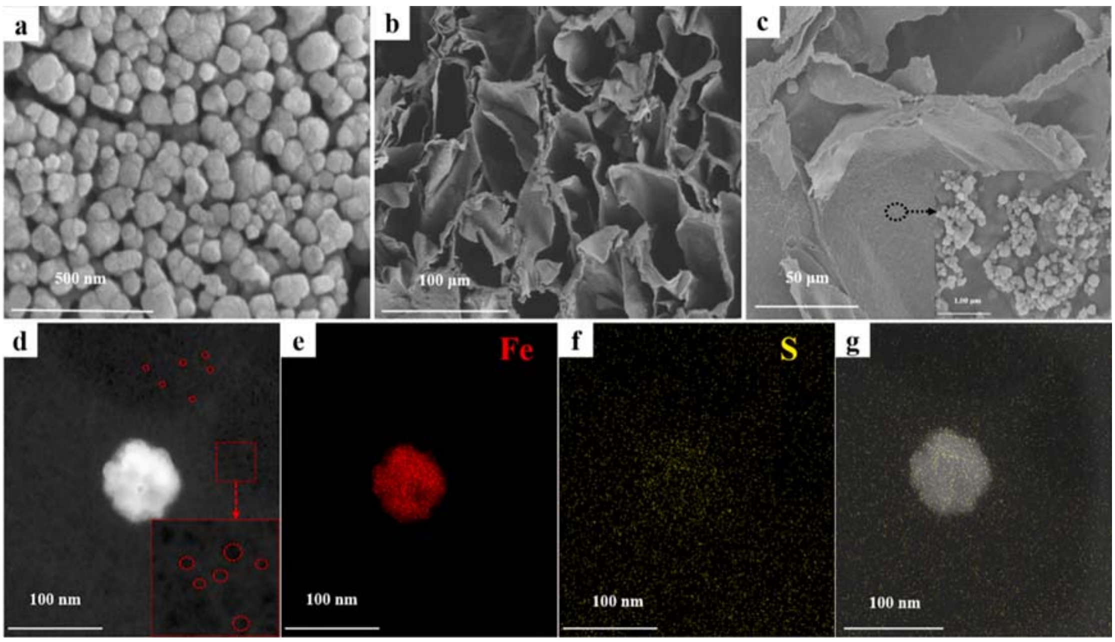

Fig. 2. SEM images of (a) PBNPs, (b) PEDOT:PSS/DF/PB hydrogel, and (c) The PEDOT:PSS/DF/PB hydrogel magnification images on the silicon wafer (inset: magnification of PBNPs on the PEDOT:PSS/DF hydrogel. TEM mappings of (d) PEDOT:PSS/DF/PB hydrogel, (e) Fe element mapping of a PBNP in the PEDOT:PSS/DF/PB hydrogel, (f) S element distribution of PEDOT in the PEDOT:PSS/DF/PB hydrogel and (g) superposition distribution of PBNPs and S element in the PEDOT:PSS/DF/PB hydrogel.

image of PEDOT:PSS/DF/PB hydrogel, it could be found that the honeycombed nanosheets of PEDOT:PSS hydrogel showed the nanonet structures as shown in Fig. 2d with red circles, which may be beneficial for the electron transfer. It also showed the PBNPs with size of 50 nm were immobilized on the hydrogel surface (white part). However, the control experiment at the absence of DMSO did no show the honeycombed structure (Fig. S2a and S2b, Supporting Information), indication the importance of DMSO and Zonyl FS-300 for the formation of porous structure. In Fig. 2e, the Fe element mapping appeared at the position of PBNP which also verified the constitute of Prussian blue. In addition, element S mapping distributed around all the image due to the presence of PEDOT on the nanosheets in Fig. 2f. The superposition imaging of PBNP and the S element in Fig. 2g indicated the existence of PBNP and PEDOT in the PEDOT:PSS/DF/PB hydrogel.

3.2. The electrochemical behaviors of PEDOT:PSS/DF/PB/GCE

The electrochemical behavior of PEDOT:PSS/DF/PB GCE electrode were investigated and compared with bare GCE, PB/GCE and PEDOT:PSS/PB/GCE electrodes, where 5 wt% of PBNPs were used on the modified electrodes. The CV measurements of these electrodes were carried out in 10 mM $K_3Fe(CN)_6$ solution as shown in Fig. 3a. The results showed the negligible current intensity for GCE and PB/GCE electrodes as compared with the PEDOT:PSS/PB/GCE and PEDOT:PSS/DF/PB/GCE electrodes. The current intensity of PEDOT:PSS/DF/PB/GCE electrode showed about 2.3 times higher current intensity than that of PEDOT:PSS/PB/GCE electrode, indicating the improvement of electrocatalytic activity upon the addition of DMSO and Zonyl FS-300. EIS measurements were also applied to characterize the charge transfer resistance (R_{ct}) of the electrodes in 5 mM $[Fe(CN)_6]^{4-/3-}$ solution containing 0.1 M KCl (Fig. 3b). The R_{ct} values were estimated with Zview software based on the classical Randles circuit as equivalent circuit in the inset of Fig. 3b. In the circuit, the R_s is the solution resistance, *C* is the capacitance, while *CPE* is represented to the diffusion impedance. The R_{ct} values were fitted as 173.2 Ω, 176 Ω, 159 Ω and 108.7 Ω for bare GCE, PB/GCE, PEDOT:PSS/PB/GCE and PEDOT:PSS/DF/PB/GCE, respectively. The R_{ct} value increased after the modification of PBNPs on the GCE electrode due to the weak conductivity of PBNPs which blocked the electronic transfer. It decreased after the modification of PEDOT:PSS/PB and the PEDOT:PSS/DF/PB on the GCE due to the well conductivity of PEDOT:PSS and better expanded polymer upon the addition of DMSO and Zonyl FS-300. Furthermore, the PEDOT:PSS hydrogel formed the well-defined pore nanostructures which was also crucial for the improvement on the electron transfer as shown in Fig. 2b.

In addition, the stability of different electrodes was investigated by 100 cycles of CV scan. As shown in Fig. 3c-e, the oxidation peak intensities of PBNPs on the PB/GCE, PEDOT:PSS/PB/GCE and PEDOT:PSS/DF/PB/GCE electrodes were reduced by 73.3%, 35.06% and 10.9% after 100 cycles of CV scan compared with 1st CV respectively. In Fig. 3f, it illustrated the PEDOT:PSS/DF/PB/GCE electrode showed significant improved stability as compared with other two electrodes. This may be also ascribed to the well expanding of PEDOT:PSS polymer and cross-linked matrix at the presence of DMSO and Zonyl FS-300, thus provided homogenous electrostatic force for the stable immobilization of PBNPs. Furthermore, the PEDOT:PSS/PB and PEDOT:PSS/DF/PB hydrogel were compared at the wet and dry state for the investigation of the stability of hydrogels. As indicated in Fig. S3, Supporting Information, the PEDOT:PSS/PB film was broken into pieces after dried while the PEDOT:PSS/DF/PB hydrogel still kept intact.

3.3. The optimization of PBNPs content on the GCE

To optimize the catalytic activity of the electrode, the PEDOT:PSS/DF/PB/GCE electrodes were prepared with different mass of PBNPs from 2.5%, 5%, 10% to 15% for the investigation of the sensitivity to H_2O_2 catalysis. The amperometric measurement of four different PEDOT:PSS/DF/PB/GCE electrodes were carried out upon the successive addition of 10 μM H_2O_2 in the PBS solution in Fig. 4a. The current

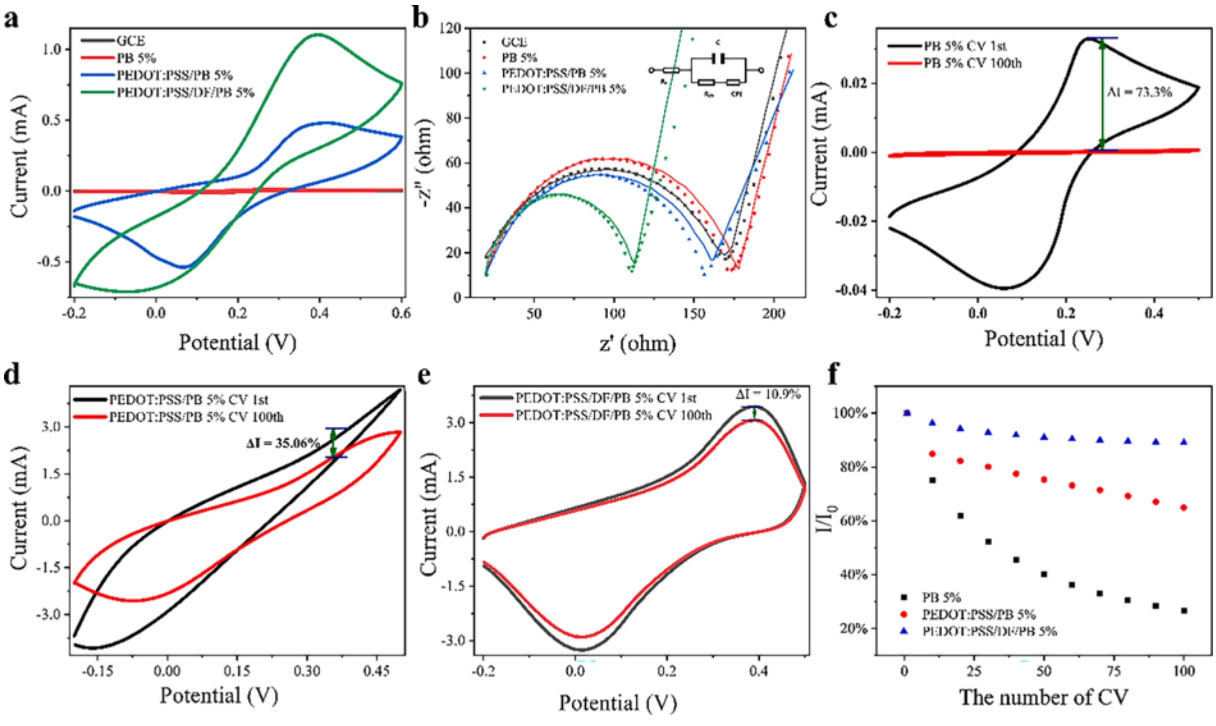

Fig. 3. (a) CV curves of bare GCE, PB/GCE, PEDOT:PSS/PB/GCE and PEDOT:PSS/DF/PB/GCE measured in 10 mM $K_3Fe(CN)_6$. (b) EIS measurements (dots) and corresponding fitting curves (solid lines) of bare GCE, PB/GCE, PEDOT:PSS/PB/GCE and PEDOT:PSS/DF/PB/GCE (inset: the classical Randles circuit) in 5 mM $[Fe(CN)_6]^{4-/3-}$ solution containing 0.1 M KCl. The 1st and 100th CVs of (c) PB/GCE, (d) PEDOT:PSS/PB/GCE and (e) PEDOT:PSS/DF/PB/GCE electrode measured in 0.05 M PBS solution (pH = 7.4), respectively. (f) The intensity ratio of oxidation peaks current changes with the numbers of CV scan circles.

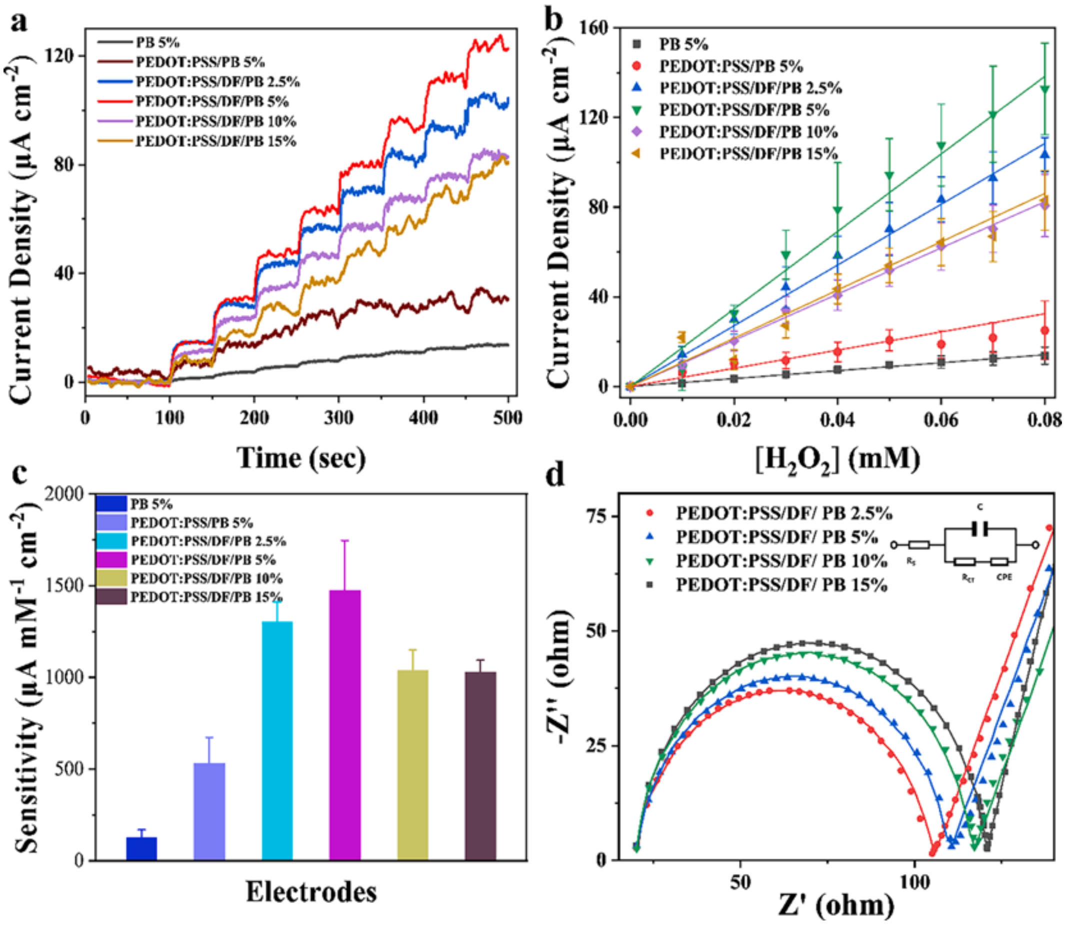

Fig. 4. (a) Amperometric responses of 6 different electrodes (PB GCE, PEDOT:PSS/PB GCE with PBNPs 5.0 wt%, PEDOT:PSS/DF/PB GCE with PBNPs 2.5 wt%, 5 wt %, 10 wt%, and 15 wt%) upon the successive addition of 10 μM H_2O_2 as measured in 0.05 M PBS (pH = 7.4) under −0.05 V of working potential. (b) The calibration curves and (c) sensitivity of these electrodes in (a) for the H_2O_2 detection. (d) EIS spectrums (dots) and corresponding fitting curves (solid lines) of PEDOT:PSS/DF/ PB GCE electrodes with different amount of PBNPs from 2.5 wt%, 5 wt%, 10 wt% to 15 wt%.

density was increased within 5 s upon the addition of 10 μM H_2O_2 in the PBS. It could be found that the PEDOT:PSS/DF/PB GCE sensor with 5 wt % PBNPs exhibited the highest current density response, while the PEDOT:PSS/DF/PB/GCE with 15 wt% PBNPs showed the lower sensitivity. It should be ascribed to the weak conductivity of PBNPs which hinders the electronic transport on the GCE surface with high amount of PBNPs. In Fig. 4a, the PEDOT:PSS/PB and PB GCE demonstrated less current response as compared with PEDOT:PSS/DF/PB GCE electrodes. This might be the weak stability of the PEDOT:PSS film without the efficient expanding of polymer or the presence of high amount of PBNPs which reduced the hydrogel stability and conductivity. In Fig. 4b, the calibration curves of six electrodes demonstrated good linearities of the current density changes to H_2O_2 concentration from 0 to 0.08 mM, with the highest sensitivity of 1474.0 $\mu A \cdot mM^{-1} \cdot cm^{-2}$ for PEDOT:PSS/DF/PB GCE with 5 wt% of PBNPs as shown in Fig. 4c. The sensitivity is about 11-fold higher than PB GCE (129.5 $\mu A \cdot mM^{-1} \cdot cm^{-2}$), and about 2.7-fold higher than the PEDOT:PSS/PB/GCE with 5.0 wt% PBNPs (531.1 $\mu A \cdot mM^{-1} \cdot cm^{-2}$). The EIS measurements were also applied for the investigation of charge transfer resistance for PEDOT:PSS/DF/PB GCE electrodes at different amount of PBNPs in Fig. 4d. The R_{ct} of the electrodes increased proportionally to the amount of PBNPs (from 2.5% to 15%) as 103.2 Ω, 107.5 Ω, 112.9 Ω and 114.5 Ω, respectively. It has to be noted that the higher amount of PBNPs may improve the sensitivity for H_2O_2 catalysis but also hinder the electron transfer and weaken the stability of the hydrogel. Therefore, the optimal amount of 5 wt% PBNPs was considered for the construction of the electrode on the following glucose sensing.

3.4. The optimization of GOx modified PEDOT:PSS/DF/PB electrode

Glucose oxidase (GOx) is typically applied in the glucose sensors, however, its activity may be affected by the surrounding environment such as pH, humidity, solvent, temperature and so on. In order to maintain the enzymatic activity, the solvent DMSO was removed after the formation of PEDOT:PSS/DF/PB hydrogel, and the pH value of the hydrogel was adjusted to investigate the optimal activity. The FT-IR spectra was employed for the characterization of DMSO, FS300, PEDOT:PSS/DF/PB solution and dried PEDOT:PSS/DF/PB hydrogel in Fig. S4, Supporting Information. Noted that DMSO showed the stretching and bending vibration peak of sulfoxyl group at 1024 cm^{-1} and 950 cm^{-1}, and stretching vibration of methyl group at 3000 and 2,910 cm^{-1} [35]. The Zonyl FS-300 showed the characteristic peak at 1105 cm^{-1}, 1230 cm^{-1} and 2865 cm^{-1} assigned to the stretching vibration of C-F, C-O, and –CH_2-, respectively [44]. Furthermore, the PEDOT:PSS/DF/PB solution exhibited the stretching vibration peak of DMSO sulfoxyl group at 1024 cm^{-1}, which disappeared after drying due to the evaporation of DMSO. Meanwhile, we adjusted the pH of the PEDOT:PSS/DF/PB conducting hydrogel solution (PEDOT:PSS pH = 2.3) to obtain the suitable microenvironment for keeping the enzyme activity. In Fig. 5a, the pH of PEDOT:PSS/DF/PB solution was adjusted from 4, 5, 5.5, 6 to 7.0 prior to load GOx in the PEDOT:PSS/DF/PB. The amperometric measurements of the prepared PEDOT:PSS/DF/PB/GOx electrodes was carried out upon the continuous addition of 10 μM glucose in PBS. The PEDOT:PSS/DF/PB/GOx electrode prepared at pH = 5.5 possessed the largest current response with a high sensitivity of 330 μA mM^{-1} cm^{-2} for the glucose

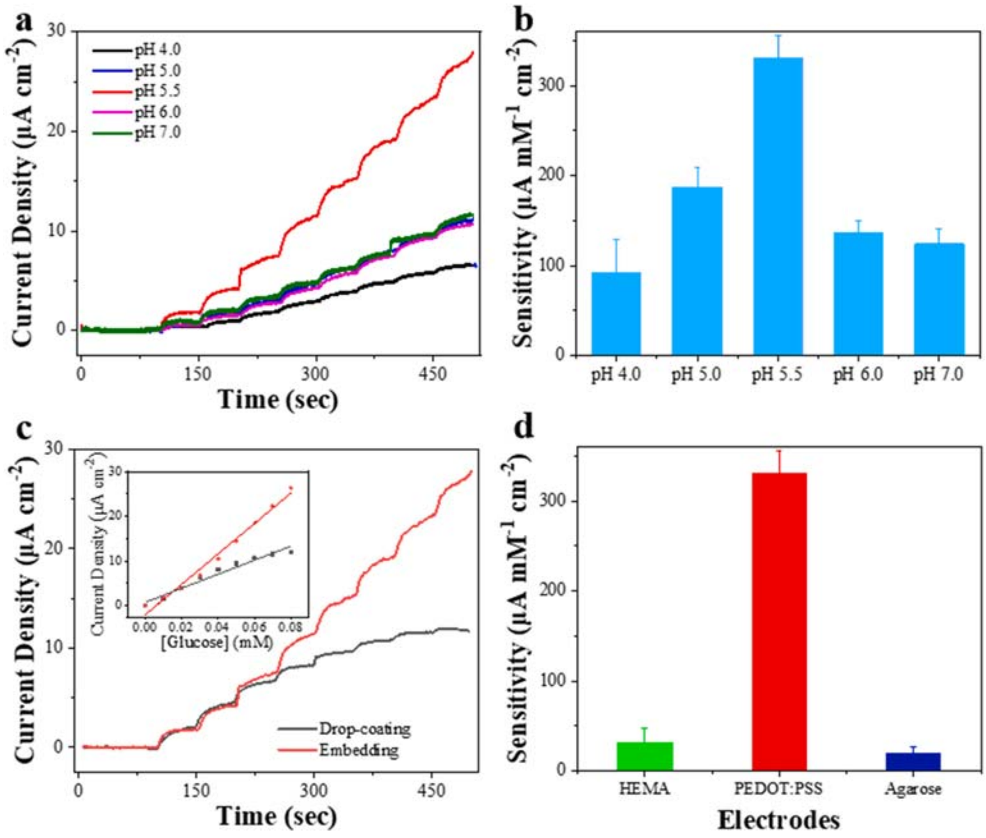

Fig. 5. (a) Amperometric measurements of PEDOT:PSS/DF/PB/GOx GCE sensor upon the continuous addition of 10 μM glucose in PBS. The PEDOT:PSS/DF/PB solution was adjusted to pH from 4, 5, 5.5, 6 to 7 prior to the load of GOx (20 mg/mL). (b) The corresponding sensitivity of the glucose biosensors based on the PEDOT:PSS/DF/PB GCE electrode prepared under different pH. (c) Amperometric measurements on the PEDOT:PSS/DF/PB (pH = 5.5) GCE electrodes prepared under embedding and drop-coating method, respectively. Inset: the corresponding calibration curves for two different loading of GOx. (d) The glucose detection sensitivity with different hydrogel sensor chips, including the HEMA/PB/GOx, PEDOT:PSS/DF/PB GOx and agarose/PB/GOx GCE.

detection in PBS, which was 2 to 3 times higher than others as shown in Fig. 5b. It indicated that the GOx demonstrated the highest catalytic activity in the acid solution such as pH = 5.5, which is consisted with the reported results [45]. In addition, we also investigated the immobilizing methods of GOx on the electrode including drop-coating and embedding of GOx in the PEDOT:PSS/DF/PB hydrogel (Fig. 5c). For the drop-coating of GOx on the electrode, the current response of the glucose sensor exhibited lower sensitivity upon the addition of glucose in the amperometric measurements. While for the embedding of GOx in the hydrogel, the current response shows constant increase upon the addition of glucose, indicating the higher sensitivity and detection range. The calibration curve on the detection of glucose shows more than 2-fold higher sensitivity (339.1 μA mM^{-1} cm^{-2}) for the enzyme embedding method than that of drop-coating method (159.6 μA mM^{-1} cm^{-2}). This might be ascribed to the homogenous and stable distribution of GOx in the polyporous PEDOT:PSS hydrogel based on enzyme embedding thus shorten electron transfer paths from the GOx active sites to the electrode. While the GOx drop-coated on the hydrogel surface might be inhomogenous and lost partially through diffusion into the electrolyte during measurement thus resulted in the poorer sensitivity.

In addition, other commonly used hydrogels such as HEMA and agarose were modified on the GCE electrode for the comparison of their sensitivities to glucose with PEDOT:PSS. These hydrogels were usually used as the skin patches for the wearable sensors, including the noninvasive interstitial fluid (ISF) glucose detection based on reverse iontophoresis [21]. With the same preparation method on the PBNPs and GOx modification, the PEDOT:PSS/DF/PB/GOx sensor obviously showed more than 10-time higher sensitivity to glucose (330 μA mM^{-1} cm^{-2}) than the HEMA (31.3 μA mM^{-1} cm^{-2}) and agarose hydrogel modified electrodes (20.0 μA mM^{-1} cm^{-2}) as shown in Fig. 5d. This should be ascribed to the high conductivity of PEDOT:PSS which improved the electron transfer between the enzyme active sites and the electrode.

Furthermore, the reproducibility of the sensors were investigated on six different PEDOT:PSS/DF/PB/GOx sensors fabricated with the same batch. All the six independent electrodes showed the high sensitivity with the relative standard deviation (RSD) down to 7.04% (Fig. S5, Supporting Information), indicating the good reproducibility. The long-term stability of the as-prepared sensor was also investigated by measuring their sensitivity repeatedly every week for one month. Note that the sensor was stored at 4℃ in the refrigerator before usage. The glucose sensor maintained 92.3% of the sensitivity upon 3 weeks storage, but decreased to 62.3% in the 4th week (Fig. S6, Supporting Information), may be ascribed to the reduced activity of enzyme.

3.5. PEDOT:PSS/DF/PB/GOx sensor for glucose sensing

The limit of detection (LOD), detection range and selectivity of the PEDOT:PSS/DF/PB/GOx sensor were further investigated in PBS. As shown in Fig. 6a, the *I-t* curve indicated the current intensity increased gradually upon the successive injection of glucose at concentrations from 1 μM, 10 μM, 100 μM to 1000 μM in PBS measured under working potential of −0.05 V. Furthermore, the current density was proportional to the glucose concentration with a sensitivity of 340.1 μA mM^{-1} cm^{-2} at the range of 1–243 μM (R^2 = 0.985) and lower sensitivity of 184.3 μA mM^{-1} cm^{-2} at high concentration range of 243–3243 μM (R^2 = 0.996) (Fig. 6b). The appearance of two linear ranges was mainly ascribed to the different enzyme activity at low and high glucose concentrations, corresponding to the first-order kinetics with high reaction rate and the zero-order kinetics with low reaction rate in the Michaelis-Menten kinetics, respectively. Besides, the high concentration of products may inhibit the reaction thus reduce the reaction sensitivity [46]. The LOD for the detection of glucose in PBS was estimated as low as 0.85 μM, (S/N = 3) as shown in Fig. 6b. In addition, the selectivity of the sensor was conducted by addition of different interferents such as AA (10 μM), UA (100 μM), NaCl (100 μM), and AP (100 μM) in the 0.05 M PBS. The interferents showed negligible current variations as compared to the

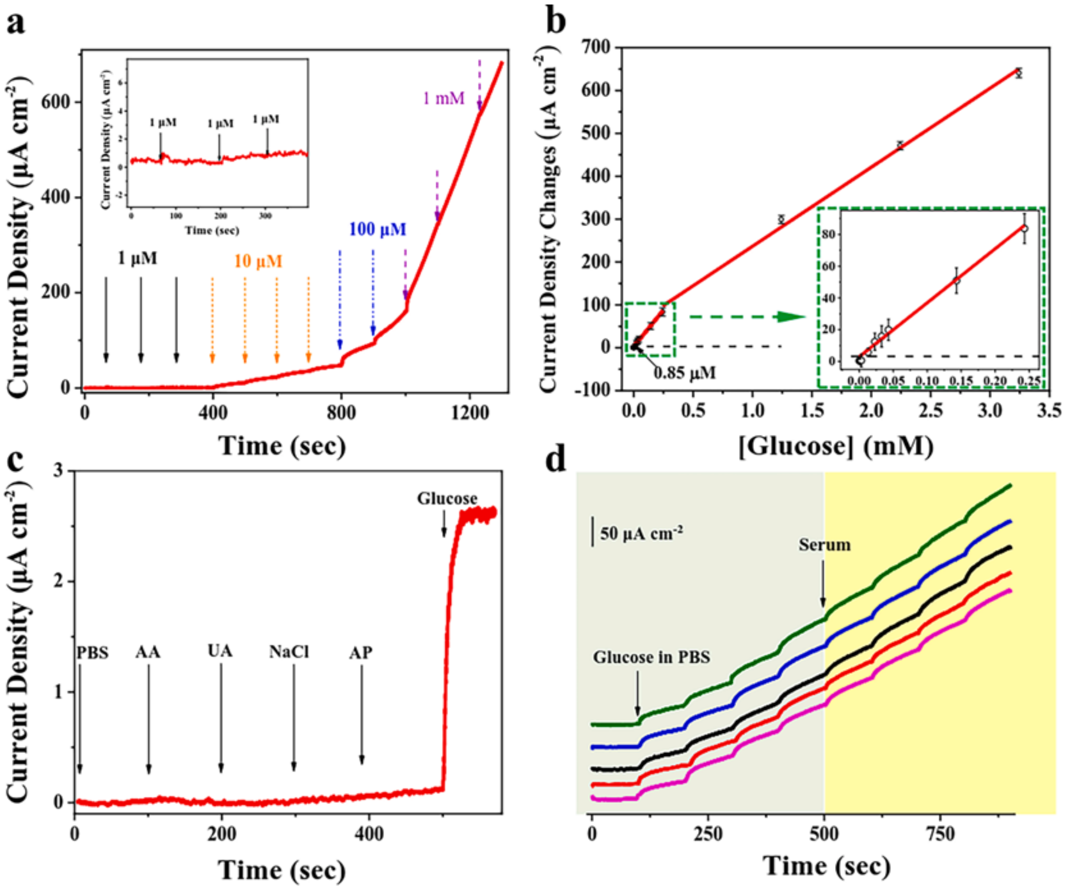

Fig. 6. (a) The current response of the as-prepared sensors upon the addition of different concentrations of glucose (1 μM, 10 μM, 100 μM to 1000 μM) in PBS at working potential of −0.05 V. (b) The calibration curve for the detection of glucose, with the error bars obtained from 3 measurements. Inset is the calibration curve for the glucose at concentrations from 0 to 0.25 mM. (c) The selectivity test of the as-prepared sensor in 0.05 M PBS (pH = 7.4) upon the addition of different interferents. (d) The amperometric responses of five different glucose sensors upon the injection of glucose (25 μM) in PBS buffer (green part) and in rabbit serum (yellow part), respectively.

response of glucose (10 μM) as observed in Fig. 6c.

The prepared glucose sensor demonstrated the high sensitivity, high linear range and low LOD as compared with other reported glucose sensors, such as PTTzFr/GOx on the graphite (LOD of 12.8 μM), GOx/Pt/rGO/ P3ABA/SPE (LOD of 44.3 μM) as concluded in Table 1. In addition, the working potential for the glucose detection was as low as −0.05 V which reduced the energy consuming and avoided the interfering signal produced by the electro-redox of some interferents such as AA, UA and so on.

3.6. Glucose detection in rabbit serum

In Fig. 6d, five independent PEDOT:PSS/DF/PB/GOx sensors were carried out for the detection of glucose with continuously addition of glucose in PBS and the original rabbit serum, respectively. In the amperometric measurements, glucose (1 M, 1 μL in PBS) with the final

Table 1
The performance comparisons with the other reported glucose sensors.

Electrodes	Potential (V)	Sensitivity (μA mM^{-1} cm^{-2})	Linear/detection range (mM)	Detection limit (μM)	Detection medium	Real sample analysis	Ref.
PTTzFr/GOx on graphite	−0.7	65.44	0.005–0.7	12.8	0.05 M PBS	beverage	[47]
SiC@C/Pt NWE/ GOx	0.6	0.02072	0–1	41	PBS	HUVECs, LO2 cells	[48]
GOx/Pt/rGO/ P3ABA/ SPE	0.5	22.01	0.25–6	44.3	0.1 M PBS pH 7.4	human serum	[49]
GOx/SPE/3D- PMED	−0.1	35.7	0–1.9	5	0.01 M PBS	sweat	[50]
GOx/Cs/PB/Au/ PET	0	2.35	0–0.2	–	PBS	sweat	[20]
GOx/PB/Au/PDMS	–	26.31	0.06–1	–	PBS	sweat	[51]
Pt@Pd/PP/LIG/GOx	0.55	247.3	0.01–9.2	3	0.1 M PBS	sweat	[52]
PET/QCS-MOxOD/GOx	0.6	176	1–111	2.4	0.1 M PBS	L929 cells	[53]
PPy/GOx/PB	0.05	2	0–2	–	phosphate buffer, pH 7.3	–	[54]
PPy/PB/Gox on graphite	0.05	1.0–1.9	0.1–20	–	phosphate buffer, pH 7.3	–	[28]
PEDOT:PSS/DF/PB/GOx GCE	−0.05 −0.05	340.1 184.3	0.001–0.243 0.243–3243	0.85	0.05 M PBS	rabbit serum	This work

concentration of 25 μM was added in the reaction solution continuously for 4 times. Similarly, the rabbit serum (200 μL) was also added for 4 times as comparison. The current intensity showed gradually increase after the injection of glucose and serum as shown in Fig. 6d. The glucose concentration in serum was accordingly estimated based on the current response and compared with the commercial glucose sensor (as summarized in Table S1, Supporting Information). The results exhibited the satisfied relative standard deviation (RSD) of lower than 6% as compared with glucometer, which was less than the deviation of 20% as regulated by the US Food and Drug Administration (FDA) for clinical blood glucose monitoring systems [55]. Therefore, we believe this biosensor provides an effective candidate for the detection of glucose in further clinical diagnosis.

3.7. On-body glucose monitoring

Further on-body glucose monitoring was carried out on two volunteers (1 male and 1 female) by attaching the hydrogel electrode on their arm and applying the reverse iontophoresis (RI) for the continuously noninvasive ISF glucose measurement (Fig. 7a, b). None of the subjects had medical history of heart disease, diabetes, or chronic skeletomuscular pain. Their blood glucose concentration was synchronously measured as comparison by glucometer with finger-stick blood sampling in 15-min before the ISF glucose extraction (Fig. 7c). The typical amperometric *I-t* measurement taken after the application of RI showed higher current density (curve b) due to the presence of ISF glucose (Fig. 7d). The difference of the current density before (curve a) and after (curve b) as shown in Fig. 7d indicated the response for ISF glucose detection. The current responses were accordingly monitored every hour for 5 and 15 h on the two volunteers underwent a snack taken similar with oral glucose tolerance test (as shown the *I-t* measurements in Figs. S7 and S8, Supporting Information), along with the blood glucose track with glucometer. The results showed that the RI-extracted ISF-borne glucose profile of the two volunteers (blue squares) matched well with that of blood glucose test (red dots) as shown in Fig. 7e and 7f. Their ISF glucose response and blood glucose increased after a snack (equally about 90 g of sugar) and reached to a maximal glucose level within 2 h followed by recovery back to the original level within 2–4 h. Note that the ISF results showed about 15-min of time lag with the blood glucose which has also been observed on previously reported articles with a typical lag of 15 min [15,22]. The time lag was ascribed to the intrinsic concentration time lag between glucose in blood and ISF. The statistical analysis of the subject 1 and 2 showed that the ISF measurement and blood results had a high correlation coefficient of 0.972 ($P < 0.005$) and 0.976 ($P < 0.001$), respectively. The current response for subject 2 plotted with the blood glucose concentration showed a good linear relation with a slope of 1.15 (Fig. 7g), indicating the good accuracy as comparison with the glucometer. In addition, there were no signs of pain or irritation on the skin surface for any of the subjects during and after the measurement. The results indicated the on-body glucose monitoring based on our PEDOT:PSS hydrogel with RI-extraction showed promising for further clinical noninvasive glucose monitoring.

4. Conclusion

In this work, PEDOT:PSS hydrogel was employed as a conductive matrix for the loading of PBNPs and GOx on GCE electrode for the electrochemical sensing of glucose. In order to obtain a high electric response, DMSO and Zonyl FS-300 were employed to better extend the PEDOT:PSS polymer chains for enhancing the electron transfer rate and improving the uniform distribution of PBNPs in the hydrogel. The PEDOT:PSS/DF/PB/GOx GCE sensor exhibited a very competitive sensitivity of 340.1 μA mM^{-1} cm^{-2} at the linear range of 1 to 243 μM and 184.3 μA mM^{-1} cm^{-2} at the linear range of 243 to 3243 μM with a low detection limit of 0.85 μM in the PBS buffer. The glucose biosensor also showed the excellent electrochemical behaviors in serum with comparable detection results compared to commercial glucometer. Importantly, we applied the glucose biosensor on two volunteers' skin surface

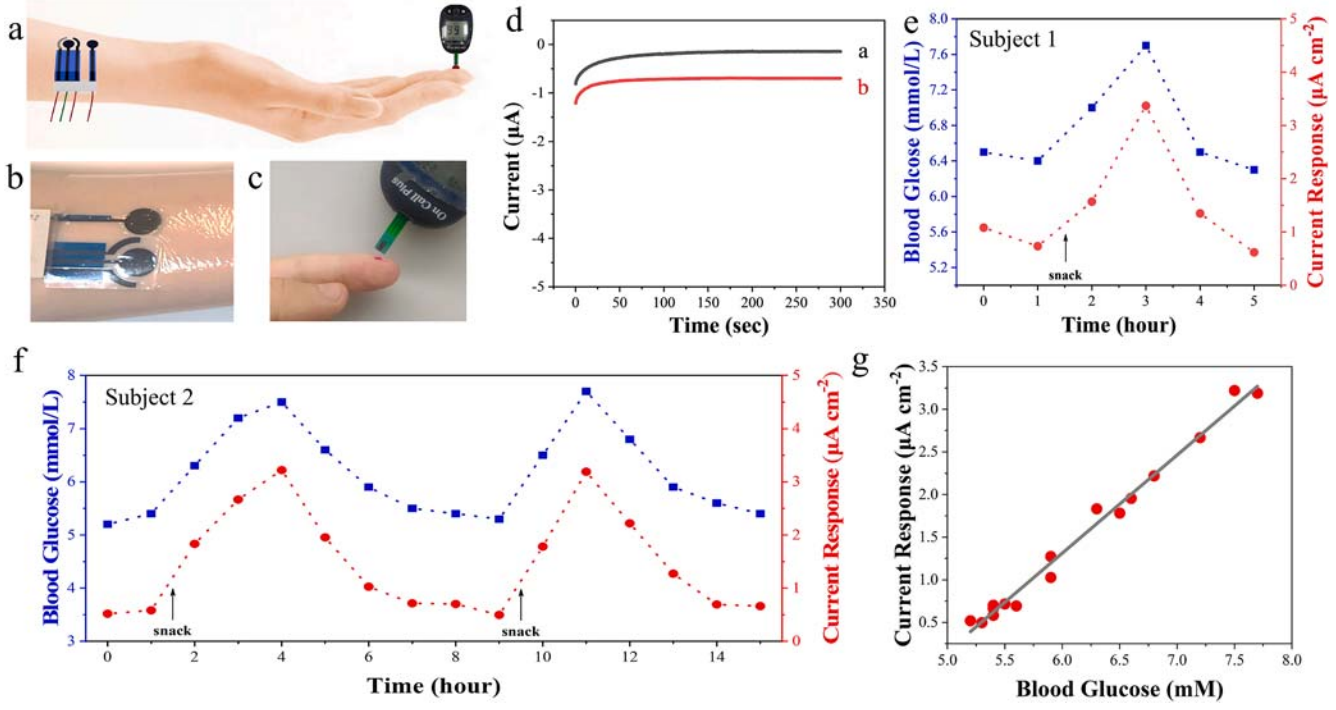

Fig. 7. (a) Schematic of the noninvasive *in vivo* glucose monitoring applied on volunteers' arm along with the synchronously finger-stick blood glucose test. (b) The SPCE electrode attached on the skin surface for the electrochemical measurement. (c) The finger-stick blood sampling for synchronously glucose measurement by glucometer. (d) Typical epidermal amperometric *I-t* measurements recorded from the sensor attached on human skin. (e, f) The noninvasive ISF glucose current response for subject 1 and 2 measured every hour versus the blood glucose measured 15-min before the ISF extraction, respectively. (g) The sensor current response versus the blood glucose concentration plotted from the data of subject 2 in (f).

and *in vivo* monitored the ISF glucose noninvasively through the RI-extraction, which showed good correlation with the finger-stick blood test by glucometer. We believe that such sensor would pave the way for the noninvasive on-body glucose monitoring in further clinical diagnosis.

Declaration of Competing Interest

The authors declare that they have no known competing financial interests or personal relationships that could have appeared to influence the work reported in this paper.

Acknowledgements

This work was financially supported by Zhejiang Province Natural Science Fund for Distinguished Young Scholars (Grant No. LR19H180001), Science and Technology Development Project of Wenzhou Longwan's (2016YG15), Leading Talent Innovation and Entrepreneurship Project of Wenzhou (RX2016005), and Publica Projects of Wenzhou (2020005).

Appendix A. Supplementary data

Supplementary data to this article can be found online at https://doi.org/10.1016/j.cej.2021.134109.

References

[1] K. Alberti, P.Z. Zimmet, W.H.O. Consultation, Definition, diagnosis and classification of diabetes mellitus and its complications part 1: Diagnosis and classification of diabetes mellitus – provisional report of a WHO consultation, Diabetic Med. 15 (7) (1998) 539–553, https://doi.org/10.1002/(sici)1096-9136(199807)15:7<539::Aid-dia668>3.0.Co;2-s.

[2] D. Jiang, Q. Zhang, C. Xu, Y. Ge, L. Huang, X. Ren, Y.i. Wang, Facile preparation of a hollow core-shell nanocomposite for the ultrasensitive sensing of glucose, Sens. Actuators, B 321 (2020) 128500, https://doi.org/10.1016/j.snb.2020.128500.

[3] D.M. Nathan, The diabetes control and complications trial/epidemiology of diabetes interventions and complications study at 30 Years: overview, Diabetes Care 37 (1) (2014) 9–16, https://doi.org/10.2337/dc13-2112.

[4] P.D. Reaven, N.V. Emanuele, W.L. Wiitala, G.D. Bahn, D.J. Reda, M. McCarren, W. C. Duckworth, R.A. Hayward, V. Investigators, Intensive glucose control in patients with type 2 diabetes-15-year follow-up, N. Engl. J. Med. 380 (23) (2019) 2215–2224, https://doi.org/10.1056/NEJMoa1806802.

[5] D. LeRoith, G.J. Biessels, S.S. Braithwaite, F.F. Casanueva, B. Draznin, J.B. Halter, I.B. Hirsch, M.E. McDonnell, M.E. Molitch, M.H. Murad, A.J. Sinclair, Treatment of diabetes in older adults: an endocrine society clinical practice guideline, J. Clin. Endocrinol. Metab. 104 (5) (2019) 1520–1574, https://doi.org/10.1210/jc.2019-00198.

[6] L. Kühner, R. Semenyshyn, M. Hentschel, F. Neubrech, C. Tarín, H. Giessen, Vibrational sensing using infrared nanoantennas: toward the noninvasive quantitation of physiological levels of glucose and fructose, ACS Sens. 4 (8) (2019) 1973–1979, https://doi.org/10.1021/acssensors.9b00488.

[7] V.P. Rachim, W.-Y. Chung, Wearable-band type visible-near infrared optical biosensor for non-invasive blood glucose monitoring, Sens. Actuators, B 286 (2019) 173–180, https://doi.org/10.1016/j.snb.2019.01.121.

[8] T.L. Chen, Y.L. Lo, C.C. Liao, Q.H. Phan, Noninvasive measurement of glucose concentration on human fingertip by optical coherence tomography, J. Biomed. Opt. 23 (4) (2018) 1–9, https://doi.org/10.1117/1.JBO.23.4.047001.

[9] A. Koh, D. Kang, Y. Xue, S. Lee, R.M. Pielak, J. Kim, T. Hwang, S. Min, A. Banks, P. Bastien, M.C. Manco, L. Wang, K.R. Ammann, K.I. Jang, P. Won, S. Han, R. Ghaffari, U. Paik, M.J. Slepian, G. Balooch, Y.G. Huang, J.A. Rogers, A soft, wearable microfluidic device for the capture, storage, and colorimetric sensing of sweat, Sci. Transl. Med. 8 (366) (2016) 13, https://doi.org/10.1126/scitranslmed.aaf2593.

[10] S.B. Kim, Y.i. Zhang, S.M. Won, A.J. Bandodkar, Y. Sekine, Y. Xue, J. Koo, S. W. Harshman, J.A. Martin, J.M. Park, T.R. Ray, K.E. Crawford, K.-T. Lee, J. Choi, R. L. Pitsch, C.C. Grigsby, A.J. Strang, Y.-Y. Chen, S. Xu, J. Kim, A. Koh, J.S. Ha, Y. Huang, S.W. Kim, J.A. Rogers, Super-absorbent polymer valves and colorimetric chemistries for time-sequenced discrete sampling and chloride analysis of sweat via skin-mounted soft microfluidics, Small 14 (12) (2018) 1703334, https://doi.org/10.1002/smll.201703334.

[11] M. Elsherif, M.U. Hassan, A.K. Yetisen, H. Butt, Wearable contact lens biosensors for continuous glucose monitoring using smartphones, ACS Nano 12 (6) (2018) 5452–5462, https://doi.org/10.1021/acsnano.8b00829.

[12] W.X. Han, H.X. He, L.L. Zhang, C.Y. Dong, H. Zeng, Y.T. Dai, L.L. Xing, Y. Zhang, X. Y. Xue, A self-powered wearable noninvasive electronic-skin for perspiration analysis based on piezo-biosensing unit matrix of enzyme/ZnO nanoarrays, ACS Appl. Mater. Interfaces 9 (35) (2017) 29526–29537, https://doi.org/10.1021/acsami.7b07990.

[13] J.W. Kang, Y.S. Park, H. Chang, W. Lee, S. Singh, W. Choi, L.H. Galindo, R. R. Dasari, S.H. Nam, J. Park, P.T.C. So, Direct observation of glucose fingerprint using in vivo Raman spectroscopy, Sci. Adv. 6 (4) (2020) 8, https://doi.org/10.1126/sciadv.aay5206.

[14] T. Yilmaz, R. Foster, Y. Hao, Radio-frequency and microwave techniques for non-invasive measurement of blood glucose levels, Diagnostics 9 (1) (2019) 6, https://doi.org/10.3390/diagnostics9010006.

[15] Y. Chen, S. Lu, S. Zhang, Y. Li, Z. Qu, Y. Chen, B. Lu, X. Wang, X. Feng, Skin-like biosensor system via electrochemical channels for noninvasive blood glucose monitoring, Sci. Adv. 3 (12) (2017), e1701629, https://doi.org/10.1126/sciadv.1701629.

[16] J. Kim, A.S. Campbell, B.E.F. de Avila, J. Wang, Wearable biosensors for healthcare monitoring, Nat. Biotechnol. 37 (4) (2019) 389–406, https://doi.org/10.1038/s41587-019-0045-y.

[17] S. Kusama, K. Sato, Y. Matsui, N. Kimura, H. Abe, S. Yoshida, M. Nishizawa, Transdermal electroosmotic flow generated by a porous microneedle array patch, Nat. Commun. 12 (1) (2021) 11, https://doi.org/10.1038/s41467-021-20948-4.

[18] H. Lee, Y.J. Hong, S. Baik, T. Hyeon, D.-H. Kim, Enzyme-based glucose sensor: from invasive to wearable device, Adv. Healthc. Mater. 7 (8) (2018) 1701150, https://doi.org/10.1002/adhm.201701150.

[19] Y. Yang, W. Gao, Wearable and flexible electronics for continuous molecular monitoring, Chem. Soc. Rev. 48 (6) (2019) 1465–1491, https://doi.org/10.1039/c7cs00730b.

[20] W. Gao, S. Emaminejad, H.Y.Y. Nyein, S. Challa, K. Chen, A. Peck, H.M. Fahad, H. Ota, H. Shiraki, D. Kiriya, D.H. Lien, G.A. Brooks, R.W. Davis, A. Javey, Fully integrated wearable sensor arrays for multiplexed in situ perspiration analysis, Nature 529 (7587) (2016) 509–514, https://doi.org/10.1038/nature16521.

[21] A.J. Bandodkar, W. Jia, C. Yardımcı, X. Wang, J. Ramirez, J. Wang, Tattoo-based noninvasive glucose monitoring: a proof-of-concept study, Anal. Chem. 87 (1) (2014) 394–398, https://doi.org/10.1021/ac504300n.

[22] L. Lipani, B.G.R. Dupont, F. Doungmene, F. Marken, R.M. Tyrrell, R.H. Guy, A. Ilie, Non-invasive, transdermal, path-selective and specific glucose monitoring via a graphene-based platform, Nat. Nanotechnol. 13 (6) (2018) 504–511, https://doi.org/10.1038/s41565-018-0112-4.

[23] J. Kim, A.S. Campbell, J. Wang, Wearable non-invasive epidermal glucose sensors: a review, Talanta 177 (2018) 163–170, https://doi.org/10.1016/j.talanta.2017.08.077.

[24] W. Chen, S. Cai, Q.Q. Ren, W. Wen, Y.D. Zhao, Recent advances in electrochemical sensing for hydrogen peroxide: a review, Analyst 137 (1) (2012) 49–58, https://doi.org/10.1039/c1an15738h.

[25] A.A. Karyakin, Advances of Prussian blue and its analogues in (bio)sensors, Curr. Opin. Electrochem. 5 (1) (2017) 92–98, https://doi.org/10.1016/j.coelec.2017.07.006.

[26] M. Li, Z. Wang, J. Liang, H. Yao, L. Shen, H. Liu, L. Fan, A chemical/molecular 4-input/2-output keypad lock with easy resettability based on red-emission carbon dots-Prussian blue composite film electrodes, Nanoscale 10 (16) (2018) 7484–7493, https://doi.org/10.1039/c8nr01258j.

[27] Z. Chu, Y. Liu, W. Jin, Recent progress in Prussian blue films: Methods used to control regular nanostructures for electrochemical biosensing applications, Biosens. Bioelectron. 96 (2017) 17–25, https://doi.org/10.1016/j.bios.2017.04.036.

[28] A. Ramanavicius, A.I. Rekertaitė, R. Valiūnas, A. Valiūnienė, Single-step procedure for the modification of graphite electrode by composite layer based on polypyrrole, Prussian blue and glucose oxidase, Sens. Actuators, B 240 (2017) 220–223, https://doi.org/10.1016/j.snb.2016.08.142.

[29] X. Yu, J.Y. Liang, T.G. Yang, M.J. Gong, D.M. Xi, H.Y. Liu, A resettable and reprogrammable keypad lock based on electrochromic Prussian blue films and biocatalysis of immobilized glucose oxidase in a bipolar electrode system, Biosens. Bioelectron. 99 (2018) 163–169, https://doi.org/10.1016/j.bios.2017.07.054.

[30] Q. Zhang, D. Jiang, C. Xu, Y. Ge, X. Liu, Q. Wei, L. Huang, X. Ren, C. Wang, Y. i. Wang, Wearable electrochemical biosensor based on molecularly imprinted Ag nanowires for noninvasive monitoring lactate in human sweat, Sens. Actuators, B 320 (2020) 128325, https://doi.org/10.1016/j.snb.2020.128325.

[31] M. Pumera, A. Ambrosi, A. Bonanni, E.L.K. Chng, H.L. Poh, Graphene for electrochemical sensing and biosensing, TrAC, Trends Anal. Chem. 29 (9) (2010) 954–965, https://doi.org/10.1016/j.trac.2010.05.011.

[32] G.A. Rivas, M.D. Rubianes, M.C. Rodríguez, N.F. Ferreyra, G.L. Luque, M. L. Pedano, S.A. Miscoria, C. Parrado, Carbon nanotubes for electrochemical biosensing, Talanta 74 (3) (2007) 291–307, https://doi.org/10.1016/j.talanta.2007.10.013.

[33] X. Fan, W. Nie, H. Tsai, N. Wang, H. Huang, Y. Cheng, R. Wen, L. Ma, F. Yan, Y. Xia, PEDOT:PSS for flexible and stretchable electronics: modifications, strategies, and applications, Adv. Sci. 6 (19) (2019) 1900813, https://doi.org/10.1002/advs.201900813.

[34] S. Ramanavicius, A. Ramanavicius, Charge transfer and biocompatibility aspects in conducting polymer-based enzymatic biosensors and biofuel cells, Nanomaterials 11 (2) (2021) 371, https://doi.org/10.3390/nano11020371.

[35] B. Lu, H. Yuk, S. Lin, N. Jian, K. Qu, J. Xu, X. Zhao, Pure PEDOT:PSS hydrogels, Nat. Commun. 10 (1) (2019) 1043, https://doi.org/10.1038/s41467-019-09003-5.

[36] Y. van de Burgt, E. Lubberman, E.J. Fuller, S.T. Keene, G.C. Faria, S. Agarwal, M. J. Marinella, A. Alec Talin, A. Salleo, A non-volatile organic electrochemical device as a low-voltage artificial synapse for neuromorphic computing, Nature Mater 16 (4) (2017) 414–418.

[37] J. Zhou, Y.-L. Hsieh, Conductive polymer protonated nanocellulose aerogels for tunable and linearly responsive strain sensors, ACS Appl. Mater. Interfaces 10 (33) (2018) 27902–27910, https://doi.org/10.1021/acsami.8b10239.
[38] Y. Ding, J. Yang, C.R. Tolle, Z. Zhu, Flexible and compressible PEDOT:PSS@ Melamine conductive sponge prepared via one-step dip coating as piezoresistive pressure sensor for human motion detection, ACS Appl. Mater. Interfaces 10 (18) (2018) 16077–16086, https://doi.org/10.1021/acsami.8b00457.
[39] J.W. Lee, D.C. Han, H.J. Shin, S.H. Yeom, B.K. Ju, W. Lee, PEDOT:PSS-based temperature-detection thread for wearable devices, Sensors 18 (9) (2018), https://doi.org/10.3390/s18092996.
[40] H. Yuk, B. Lu, S. Lin, K. Qu, J. Xu, J. Luo, X. Zhao, 3D printing of conducting polymers, Nat. Commun. 11 (1) (2020) 1604, https://doi.org/10.1038/s41467-020-15316-7.
[41] L. Manjakkal, A. Pullanchiyodan, N. Yogeswaran, E.S. Hosseini, R. Dahiya, A Wearable supercapacitor based on conductive PEDOT:PSS-coated cloth and a sweat electrolyte, Adv. Mater. 32 (24) (2020) 1907254, https://doi.org/10.1002/adma.201907254.
[42] D. Jiang, Z. Chu, J. Peng, W. Jin, Screen-printed biosensor chips with Prussian blue nanocubes for the detection of physiological analytes, Sens. Actuators, B 228 (2016) 679–687, https://doi.org/10.1016/j.snb.2016.01.076.
[43] J. Deng, S. Chen, J. Chen, H. Ding, D. Deng, Z. Xie, Self-reporting colorimetric analysis of drug release by molecular imprinted structural color contact lens, ACS Appl Mater Interfaces 10 (40) (2018) 34611–34617, https://doi.org/10.1021/acsami.8b11655.
[44] S. Zanini, L. Zoia, E.C. Dell'Orto, A. Natalello, A.M. Villa, R.D. Pergola, C. Riccardi, Plasma polymerized 2-ethyl-2-oxazoline: Chemical characterization and study of the reactivity towards different chemical groups, Mater. Des. 108 (2016) 791–800, https://doi.org/10.1016/j.matdes.2016.07.051.
[45] F.K. Derakshan, F. Darvishi, M. Dezfulian, C. Madzak, Expression and characterization of glucose oxidase from Aspergillus niger in Yarrowia lipolytica, Mol. Biotechnol. 59 (8) (2017) 307–314, https://doi.org/10.1007/s12033-017-0017-8.
[46] C. Garcia-Galan, Á. Berenguer-Murcia, R. Fernandez-Lafuente, R.C. Rodrigues, Potential of different enzyme immobilization strategies to improve enzyme performance, Adv. Synth. Catal. 353 (16) (2011) 2885–2904, https://doi.org/10.1002/adsc.201100534.
[47] S. Soylemez, H.Z. Kaya, Y.A. Udum, L. Toppare, A multipurpose conjugated polymer: Electrochromic device and biosensor construction for glucose detection, Org. Electron. 65 (2019) 327–333, https://doi.org/10.1016/j.orgel.2018.11.001.
[48] Q.L. Liao, H. Jiang, X.W. Zhang, Q.F. Qiu, Y. Tang, X.K. Yang, Y.L. Liu, W. H. Huang, A single nanowire sensor for intracellular glucose detection, Nanoscale 11 (22) (2019) 10702–10708, https://doi.org/10.1039/c9nr01997a.
[49] S. Phetsang, J. Jakmunee, P. Mungkornasawakul, R. Laocharoensuk, K. Ounnunkad, Sensitive amperometric biosensors for detection of glucose and cholesterol using a platinum/reduced graphene oxide/poly(3-aminobenzoic acid) film-modified screen-printed carbon electrode, Bioelectrochemistry 127 (2019) 125–135, https://doi.org/10.1016/j.bioelechem.2019.01.008.
[50] Q. Cao, B. Liang, T. Tu, J. Wei, L. Fang, X. Ye, Three-dimensional paper-based microfluidic electrochemical integrated devices (3D-PMED) for wearable electrochemical glucose detection, RSC Adv. 9 (10) (2019) 5674–5681, https://doi.org/10.1039/C8RA09157A.
[51] M.A. Yokus, T. Songkakul, V.A. Pozdin, A. Bozkurt, M.A. Daniele, Wearable multiplexed biosensor system toward continuous monitoring of metabolites, Biosens. Bioelectron 153 (2020) 112038, https://doi.org/10.1016/j.bios.2020.112038.
[52] M.A. Zahed, S.C. Barman, P.S. Das, M.d. Sharifuzzaman, H.S. Yoon, S.H. Yoon, J. Y. Park, Highly flexible and conductive poly (3, 4-ethylene dioxythiophene)-poly (styrene sulfonate) anchored 3-dimensional porous graphene network-based electrochemical biosensor for glucose and pH detection in human perspiration, Biosens. Bioelectron 160 (2020) 112220, https://doi.org/10.1016/j.bios.2020.112220.
[53] Z. Liang, J. Zhang, C. Wu, X. Hu, Y. Lu, G. Wang, F. Yu, X. Zhang, Y. Wang, Flexible and self-healing electrochemical hydrogel sensor with high efficiency toward glucose monitoring, Biosens. Bioelectron 155 (2020) 112105, https://doi.org/10.1016/j.bios.2020.112105.
[54] A.I. Rekertaitė, A. Valiūnienė, P. Virbickas, A. Ramanavicius, Physicochemical characteristics of polypyrrole/(glucose oxidase)/(prussian blue)-based biosensor modified with Ni- and Co-hexacyanoferrates, Electroanalysis 31 (1) (2019) 50–57, https://doi.org/10.1002/elan.201800526.
[55] J.A. DuBois, R.J. Slingerland, M. Fokkert, A. Roman, N.K. Tran, W. Clarke, D. A. Sartori, T.L. Palmieri, A. Malic, M.E. Lyon, A.W. Lyon, Bedside glucose monitoring-is it safe? a new, regulatory-compliant risk assessment evaluation protocol in critically ill patient care settings, Crit. Care Med. 45 (4) (2017) 567–574, https://doi.org/10.1097/CCM.0000000000002252.